Nucleon spin structure functions, considering target mass correction, and higher twist effects at the NNLO accuracy and their transverse momentum dependence

Abolfazl Mirjalili[1,*] and Shahin Atashbar Tehrani[2,†]

[1]*Physics Department, Yazd University, P.O. Box 89195-741, Yazd, Iran*
[2]*School of Particles and Accelerators, Institute for Research in Fundamental Sciences (IPM), P.O. Box 19395-5531, Tehran, Iran*

(Received 14 February 2022; accepted 28 March 2022; published 25 April 2022)

Using recent and updated world data on polarized structure functions g_1 and g_2 we perform an analysis based on quantum chromodynamics (QCD) as a theory of strong interactions at next-next-to-leading-order accuracy. We include also target mass corrections and higher twist effects to get more precise results in our fitting procedure. To confirm the validity of our fitting results several sum rules are examined and we do a comparison for them with results from other models. In our analysis we employ the Jacobi polynomials approach to obtain analytical solutions of the Dokshitzer-Gribov-LipatovAltarelli-Parisi evolution equations for parton distribution functions (PDFs). Using the extracted PDFs from our data analysis as input, we also compute the x- and $\mathbf{p}_T$-dependence of some transverse momentum dependence PDFs in polarized case, based on covariant parton model. These functions are naively even time-reversal at twist-two approximation. The results for transverse momentum dependences indicate proper and acceptable behavior with respect to what are presented in other literatures.

DOI: 10.1103/PhysRevD.105.074023

I. INTRODUCTION

The determination of the nucleon's spin into its quark and gluon components is still an important challenge in particle physics. The deep-inelastic scattering (DIS) experiments performed at DESY, SLAC, CERN, and JLAB have refined our understanding of the spin distributions and revealed the spin-dependent structure functions of the nucleon. The polarized structure functions $g_1(x, Q^2)$ and $g_2(x, Q^2)$ are measured in deep-inelastic scattering of a longitudinally polarized lepton on polarized nuclear targets. We do the required analysis on the polarized structure function to extract the desired parton densities at the initial energy scale, Q_0.

In exact consideration of inclusive processes it is required to take into account the distributions in which the role of transverse momentum is embedded. These distributions are known as transverse momentum dependent (TMD) distributions. TMDs are the generalization of PDFs which provide us an extensive knowledge to investigate the hadron structure function. In a native parton model in which the effect of transverse momentum of a quark is not outstanding, there is a proper computational frame which is called the infinite momentum frame (IMF) [1,2]. In this frame the target (nucleon) is moving fast, comparable to speed of light and because of Lorentz contraction the nucleon seems like a flat disc. In this case one can imagine a transverse space position of quark inside the disk with respect to the moving direction of the target. This space coordinate is called the impact parameter and is denoted usually by b_T. Corresponding to the impact parameter in coordinate space we can attribute to a quark inside the target a transverse momentum, k_T, that is perpendicular to moving direction of nucleon. This momentum component is ignorable against the quark longitudinal momentum. This model then gives oversimplified relations between structure and distribution functions. In an another model, which is called the covariant parton model (CPM) [3], more exact but much more complex relations between structure and distribution functions are given. The original assumptions of this model are based on covariance of relations together with a spherically symmetric quark momenta distribution in the nucleon rest frame where one photon exchange is used in a charged lepton-quark interaction. The output of this model is such that the quark transverse momentum is as important as the longitudinal one and the transverse momentum dependences of parton densities are obtained analytically [4].

*Corresponding author.
A.Mirjalili@yazd.ac.ir
†Atashbar@ipm.ir

The extended PDF is then describing the parton distribution with respect to both x and k_T variables. In other words quarks can have transverse momentum with respect to the motion of the parent hadron. The transverse momentum of parton at initial state and inside the parent hadron is called the intrinsic transverse momentum, denoted by k_T. In the final state the transverse momentum of parton with respect to the momentum of produced hadron is denoted by p_T. TMDs have outstanding effect on the momentum feature of produced hadron. They also have a crucial role to describe the spin asymmetry in produced hadron [5] by analysing the semi inclusive DIS (SIDIS) processes [6,7]. To achieve the three dimensional (3D) picture of nucleon, some processes like SIDIS are required in which one can measure the effect of transverse momentum of partons in created hadron. It is therefore required to consider the spin dependence of PDFs. Early applications to polarized structure functions were made by [8–10].

The PDFs in the polarized case are two types. The first one is related to the longitudinal polarized quark inside the longitudinal polarized nucleon, denoted by $g_1(x)$ that is called helicity function. The second one is related to transverse polarized quark inside the transverse polarized nucleon, denoted by $h_1(x)$ and is called the transversity function. The type of polarization is determined with respect to moving direction of nucleon. If the parton transverse momentum as an extra degree of freedom is also considered then total number of PDFs, involving polarized cases, are arising to eight ones [11]. In this article the polarized TMDs which are even time reversal functions, based on the covariant parton model, are investigated.

The organization of this paper is as follows. In Sec. II an overview on theoretical aspects of polarized structure function is done. In Sec. III the theoretical framework of Jacobi polynomials approach is reviewed. Section IV is devoted to discussing the target mass correction for g_1 and g_2 structure functions. Additionally, in Sec. V the higher twist effect is demonstrated for polarized structure functions. In Sec. VI, which includes also some subsections, we illustrate our QCD data analysis which we call it as MA22 analysis. To get more validation of our MA22 results, we examine in Sec. VII several sum rules. In Sec. VIII our predictions for polarized PDFs and structure functions are presented. Using the results of our MA22 analysis, some polarized TMDs can be calculated. We do it in Sec. IX. In the last part that is Sec. X our conclusions are given.

II. LEADING TWIST SPIN DEPENDENCE OF STRUCTURE FUNCTION

To achieve the main goal of this article to calculate the polarized TMDs we first need to consider the DIS structure function in the polarized case. For this purpose linear combination of polarized parton densities and coefficient functions can be used to express the leading twist spin-dependent proton and neutron structure functions, $g_1^{\mathrm{p}}(x,Q^2)$ at the next-next-to-leading-order (NNLO) accuracy as it follows [12–14]:

$$\begin{aligned} g_1^{\mathrm{p}}(x,Q^2) = {} & \frac{1}{2}\sum_q e_q^2 \Delta q_v(x,Q^2) \otimes \left(1+\frac{\alpha_s(Q^2)}{2\pi}\Delta C_q^{(1)} + \left(\frac{\alpha_s(Q^2)}{2\pi}\right)^2 \Delta C_{ns}^{(2)}\right) \\ & + e_q^2(\Delta q_s + \Delta\overline{q_s})(x,Q^2) \otimes \left(1+\frac{\alpha_s(Q^2)}{2\pi}\Delta C_q^{(1)} + \left(\frac{\alpha_s(Q^2)}{2\pi}\right)^2 \Delta C_s^{(2)}\right) \\ & + \frac{2}{9}\left(\frac{\alpha_s(Q^2)}{2\pi}\Delta C_g^{(1)} + \left(\frac{\alpha_s(Q^2)}{2\pi}\right)^2 \Delta C_g^{(2)}\right) \otimes \Delta g(x,Q^2) \end{aligned} \tag{1}$$

Here Δq_v, Δq_s, and Δg are the polarized valence, sea, and gluon densities, respectively. The pQCD evolution kernel for PPDFs is now available at the NNLO accuracy in Ref. [15–17]. The $\Delta C_q^{(1)}$ and $\Delta C_g^{(1)}$ in Eq. (1) are denoting to the NLO spin-dependent quark and gluon hard scattering coefficients, calculable in pQCD [18]. We now apply the hard scattering coefficients, extracted at NNLO approximation. At this order the Wilson coefficients are different for quarks and antiquarks. They are presented in Eq. (1) by $\Delta C_{ns}^{(2)}$ and $\Delta C_s^{(2)}$ respectively and their analytical relations have been reported in [19]. The symbol $\otimes$ in Eq. (1) is representing typical convolution integral in Bjorken x-space.

The neutron structure function, $g_1^{\mathrm{n}}(x,Q^2)$, can be obtained from the proton one by considering isospin symmetry. Hence the deuteron structure function at leading twist would be available, utilizing the g_1^{p} and g_1^{n} structure functions such as:

$$g_1^{\tau 2(\mathrm{d})}(x,Q^2) = \frac{1}{2}\{g_1^{\mathrm{p}}(x,Q^2) + g_1^{\mathrm{n}}(x,Q^2)\} \times (1-1.5w_D), \tag{2}$$

where $w_D = 0.05 \pm 0.01$ is the probability to find the deuteron in a $D-$ state [20–22]. Using the Wandzura and Wilczek (WW) relation [23] the leading twist polarized structure function of $g_2^{\tau_2}(x,Q^2)$ can be fully determined via $g_1^{\tau_2}(x,Q^2)$ structure function:

$$g_2^{\tau_2}(x,Q^2) = g_2^{WW}(x,Q^2) = -g_1^{\tau_2}(x,Q^2) + \int_x^1 \frac{dy}{y} g_1^{\tau_2}(y,Q^2). \quad (3)$$

This relation that is in the leading twist approximation can also be used when target mass correction (TMC) is included [23].

The $g_1^{\tau_2}(x,Q^2)$ and $g_2^{\tau_2}(x,Q^2)$ structure functions at the leading twist order have valid definition in the Bjorken limit, i.e., $Q^2 \to \infty$, $x =$ fixed. But at the a moderate low Q^2 $(\sim 1\text{–}5\ \mathrm{GeV}^2)$ and $W^2(4\ \mathrm{GeV}^2 < W^2 < 10\ \mathrm{GeV}^2)$ where W^2 is the invariant mass of the hadronic system, both TMC along with higher twist corrections should be considered. We investigate them in Sec. IV and Sec. V.

The next section is devoted to illustrating the nucleon and deuteron structure functions, based on the Jacobi polynomial approach which yield us finally the evolved functions in Bjorken x-space.

III. JACOBI POLYNOMIALS EXPANSION TECHNIQUE

To achieve the nucleon structure function in Bjorken x-space we resort to a method that is based on the Jacobi polynomials expansion. Practical aspects of this method including its major advantages are presented in our previous studies [12,13,24–29]. According to this method, one can easily expand the polarized structure functions $xg_1^{\mathrm{QCD}}(x,Q^2)$, in terms of the Jacobi polynomials $\Theta_n^{\alpha,\beta}(x)$, as it follows [30–42],

$$xg_1^{\tau 2}(x,Q^2) = x^\beta (1-x)^\alpha \sum_{n=0}^{\mathrm{N_{max}}} a_n(Q^2)\Theta_n^{\alpha,\beta}(x), \quad (4)$$

where $\mathrm{N_{max}}$ is the maximum order of expansion. The parameters α and β are Jacobi polynomials free parameters which normally fixed on their best values. These parameters have to be chosen so as to achieve the fastest convergence of the series on the right-hand side of Eq. (4). In the polynomial fitting procedure, the evolution equation is combined with the truncated series to perform a direct fit to the structure functions.

The Jacobi moments, $a_n(Q^2)$ are codifying the Q^2-dependence of the polarized structure functions. The x-dependence will be provided by the weight function $w^{\alpha,\beta}(x) \equiv x^\beta(1-x)^\alpha$ and the Jacobi polynomials $\Theta_n^{\alpha,\beta}(x)$ which can be written as,

$$\Theta_n^{\alpha,\beta}(x) = \sum_{j=0}^{n} c_j^{(n)}(\alpha,\beta)x^j, \quad (5)$$

where the coefficients $c_j^{(n)}(\alpha,\beta)$ are combinations of Gamma functions in terms of n, α, and β. The above Jacobi polynomials are satisfying the following orthonormality condition:

$$\int_0^1 dx x^\beta (1-x)^\alpha \Theta_n^{\alpha,\beta}(x)\Theta_l^{\alpha,\beta}(x) = \delta_{n,l}. \quad (6)$$

Consequently the Jacobi moments, $a_n(Q^2)$, can be obtained, using the above relation such as,

$$a_n(Q^2) = \int_0^1 dx x g_1^{\tau_2}(x,Q^2)\Theta_n^{\alpha,\beta}(x) = \sum_{j=0}^{n} c_j^{(n)}(\alpha,\beta)\mathcal{M}[xg_1^{\tau_2}, j+2](Q^2), \quad (7)$$

where the Mellin transform $\mathcal{M}[xg_1^{\tau 2}, \mathrm{N}]$ is given by,

$$\mathcal{M}[xg_1^{\tau_2}, \mathrm{N}](Q^2) \equiv \int_0^1 dx x^{\mathrm{N}-2} x g_1^{\tau_2}(x,Q^2). \quad (8)$$

Using the QCD expressions for the Mellin moments, $\mathcal{M}[xg_1^{\tau_2}, \mathrm{N}](Q^2)$, the polarized structure function $xg_1^{\tau_2}(x,Q^2)$, can be constructed. Therefore, based on the method of Jacobi polynomial expansion, the $xg_1^{\tau_2}(x,Q^2)$ is given by:

$$xg_1^{\tau_2}(x,Q^2) = x^\beta(1-x)^\alpha \sum_{n=0}^{\mathrm{N_{max}}} \Theta_n^{\alpha,\beta}(x) \times \sum_{j=0}^{n} c_j^{(n)}(\alpha,\beta)\mathcal{M}[xg_1^{\tau_2}, j+2](Q^2). \quad (9)$$

By setting $N_{\max} = 9$, $\alpha = 3$, and $\beta = 0.5$, as we have shown in our previous analyses [12,13,24–29], it is possible to obtain the optimal convergence of above expansion through the whole kinematic region that is constrained by the polarized DIS data.

In the next section we improve our analysis of DIS polarized data, considering the TMC correction to the nucleon structure functions.

IV. TARGET MASS CORRECTIONS IN POLARIZED CASE

Power suppressed corrections to the structure functions can have important contributions in some kinematic regions. Hence nucleon mass correction cannot be neglected in low Q^2 region. The TMCs can be calculated via an expression which is different from higher twist (HT) effects in dynamical case. In the case of polarized structure function we follow the suggested method by Blumlein and Tkabladze [43] which is in fact the generalized one that was established by Georgi and Politzer [44] for the unpolarized structure function.

Mellin inversion to x-space or the integer moments of structure function can be used to present these corrections. Leading twist-two expression for g_1, that is containing TMC, is given explicitly by [43]:

$$\begin{aligned} g_1^{\tau_2+\mathrm{TMCs}}(x,Q^2) &= \frac{x g_1^{\tau_2}(\xi,Q^2;\mathrm{M}=0)}{\xi(1+4\mathrm{M}^2x^2/Q^2)^{3/2}} \\ &+ \frac{4\mathrm{M}^2x^2}{Q^2}\frac{(x+\xi)}{\xi(1+4\mathrm{M}^2x^2/Q^2)^2}\int_\xi^1 \frac{d\xi'}{\xi'} g_1^{\tau_2}(\xi',Q^2;\mathrm{M}=0) \\ &- \frac{4\mathrm{M}^2x^2}{Q^2}\frac{(2-4\mathrm{M}^2x^2/Q^2)}{2(1+4\mathrm{M}^2x^2/Q^2)^{5/2}} \\ &\times \int_\xi^1 \frac{d\xi'}{\xi'}\int_{\xi'}^1 \frac{d\xi''}{\xi''} g_1^{\tau_2}(\xi'',Q^2;\mathrm{M}=0). \end{aligned} \tag{10}$$

The twist-two contribution for the g_2 structure function, including TMC is similarly presented by [43]:

$$\begin{aligned} g_2^{\tau_2+\mathrm{TMCs}}(x,Q^2) &= -\frac{x g_1^{\tau_2}(\xi,Q^2;\mathrm{M}=0)}{\xi(1+4\mathrm{M}^2x^2/Q^2)^{3/2}} \\ &+ \frac{x(1-4\mathrm{M}^2x\xi/Q^2)}{\xi(1+4\mathrm{M}^2x^2/Q^2)^2}\int_\xi^1 \frac{d\xi'}{\xi'} g_1^{\tau_2}(\xi',Q^2;\mathrm{M}=0) \\ &+ \frac{3}{2}\frac{4\mathrm{M}^2x^2/Q^2}{(1+4\mathrm{M}^2x^2/Q^2)^{5/2}} \\ &\times \int_\xi^1 \frac{d\xi'}{\xi'}\int_{\xi'}^1 \frac{d\xi''}{\xi''} g_1^{\tau_2}(\xi'',Q^2;\mathrm{M}=0), \end{aligned} \tag{11}$$

Numerical illustrations for the target mass effects in g_1 and g_2 have been given in [45]. In both above equations M is the nucleon mass and ξ is called Nachtmann variable that is defined by [46]:

$$\xi = \frac{2x}{1+\sqrt{1+4\mathrm{M}^2x^2/Q^2}}. \tag{12}$$

It can be seen that by choosing the maximum value for the x-Bjorken variable, the maximum kinematic value of ξ variable would be less than unity. This means that the target mass corrected structure functions at leading twist in both the polarized and unpolarized cases, as it is expected, do not vanish at maximum $x = 1$ value.

As we referred before, in addition to target mass correction, higher twist effects would also be dominant at low Q^2 values and make a contribution to nucleon structure function in a related kinematic region. The next section is devoted to these effects.

V. TWIST-THREE CONTRIBUTION

The long-range nonperturbative multiparton correlations which have outstanding contributions at low values of Q^2 will lead to higher twist (HT) terms. A proper analysis of this effect can be found in [47]. For a developing phenomenological analysis an advantageous parametrization is made by the Braun-Lautenschlager-Manashov-Pirnay (BLMP) model [48] for HT terms. Following that HT distributions are constructed from convolution integrals that are containing light-cone wave functions. In this connection a simple model based on three valence quark and one gluon distributions with the total zero angular momentum are assumed.

Accordingly, we utilize the parametrized form, suggested by the BLMP model at the twist-three order for g_2 structure function in an initial scale Q_0 as it follows [48,49]:

$$\begin{aligned} g_2^{\tau_3}(x) = A\left[\ln(x)+(1-x)+\frac{1}{2}(1-x)^2\right] \\ + (1-x)^3[B-C(1-x)+D(1-x)^2 \\ - E(1-x)^3]. \end{aligned} \tag{13}$$

The unknown coefficients in Eq. (13) are extracted by fitting the data. Since higher twist contributions are important in a region with large-x values, a nonsinglet evolution equation is employed. The results of this approach can be compared with exact evolution equations where a gluon-quark-antiquark correlation is considered [48]. It is expected that these two results are in good agreement with each other.

The twist-three part of different spin-dependent structure functions, $g_1^{\tau_3}$ and $g_2^{\tau_3}$, are related by the following integral relation [43].

$$g_1^{\tau 3}(x,Q^2) = \frac{4x^2M^2}{Q^2}\left[g_2^{\tau 3}(x,Q^2) - 2\int_x^1 \frac{dy}{y} g_2^{\tau 3}(y,Q^2)\right], \tag{14}$$

The Q^2-dependence of the $g_2^{\tau_3}$ can be achieved within nonsinglet perturbative QCD evolution as

$$g_2^{\tau 3}(n,Q^2) = \mathcal{M}^{\mathrm{NS}}(n,Q^2) g_2^{\tau 3}(n). \tag{15}$$

Finally the spin-dependent structure functions, considering the TMCs and HT terms are given by,

$$\begin{aligned} x g_{1,2}{}^{\mathrm{Full=pQCD+TMC+HT}}(x,Q^2) \\ = x g_{1,2}^{\tau_2+\mathrm{TMCs}}(x,Q^2) + x g_{1,2}^{\tau_3}(x,Q^2). \end{aligned} \tag{16}$$

One of the particular feature of $x g_{1,2}^{\mathrm{Full}}(x,Q^2)$ function is that the twist-three term is not suppressed there by inverse powers of Q^2. Consequently, to describe this function this contribution is as important as the twist-two contribution.

Since the required theoretical inputs are accessed by us, we now can do the concerned data analysis which is done in the next section.

VI. FITTING CONTENTS IN QCD ANALYSIS

The fitting procedure, including the recent and updated data for polarized structure functions which we do in our QCD analysis, contain the following parts.

A. Parametrization

We start the QCD analysis considering the following parametrization at the initial scale of $Q_0^2 = 1$ GeV^2 where $q = \{u_v, d_v, \bar{q}, g\}$:

$$x\Delta q(x, Q_0^2) = \mathcal{N}_q \eta_q x^{a_q}(1-x)^{b_q}(1 + c_q x). \quad (17)$$

The normalization constant $\mathcal{N}_q$,

$$\mathcal{N}_q^{-1} = \left(1 + c_q \frac{a_q}{a_q + b_q + 1}\right) B(a_q, b_q + 1), \quad (18)$$

is determined such that η_q in Eq. (17) is the first moment of the polarized parton distribution functions (PPDFs). Here $B(a, b)$ is the Euler beta function. Considering SU(3) flavor symmetry, we assume $\Delta\bar{q} \equiv \Delta\bar{u} = \Delta\bar{d} = \Delta s = \Delta\bar{s}$.

The unknown free parameters can be extracted through a fit which involves a large degree of flexibility. Some of parameters can be determined via the existing constrains, as describing in below:

(i) The weak matrix elements F and D as measured in neutron and hyperon β decays [50] can be related to the first moments of the polarized valence quark densities. Considering these constrains, the numerical values $\eta_{u_v} = 0.928 \pm 0.014$ and $\eta_{d_v} = -0.342 \pm 0.018$ are obtained.

(ii) Due to the present accuracy of the data, the $c_{\bar{q}}$ and c_g parameters are set to zero. Considering nonzero values for them, there would not be observed any improvement in the fit.

(iii) The large-x behavior of the polarized sea quarks and gluons are controlled by $b_{\bar{q}}$ and b_g parameters. In a region that is dominated by the valence distributions, these parameters have large uncertainties.

(iv) Due to higher twist effect to the $g_{2,\{p,n,d\}}$ and consequently $g_{1,\{p,n,d\}}$, there are unknown parameters $\{A, B, C, D, E\}$, see Eq. (13). By a simultaneous fit to the all polarized structure function data of g_1 and g_2, these parameters can be determined.

(v) The values of some parameters are frozen in the first minimization procedure. They involve $\{\eta_{u_v}, \eta_{d_v}, c_{\bar{q}}, c_g\}$ and finally the b parameter. As demonstrated in Tables I and II the $\{b_{\bar{q}}, b_g, c_{u_v}, c_{d_v}\}$ and $\{A, B, C, D, E\}$ parameters are then fixed in the second minimization. Nine unknown parameters, including $\alpha_s(Q_0^2)$, are left which are determined in the fit. They have enough flexibility to perform a reliable fit.

(vi) The numerical value $\alpha_s(M_Z^2) = 0.112804 \pm 0.001907$ would be achieved in which we changed the energy scale in $\alpha_s(Q_0^2)$ to the Z boson mass. It is while for the present world average, the value $\alpha_s(M_Z^2) = 0.1179 \pm 8.5 \times 10^{-6}$ is reported [51].

To extract the unknown parameters, it needs access to all available concerned datasets which we describe below.

TABLE I. Final parameter values and their statistical errors at the input scale $Q_0^2 = 1$ GeV^2 determined from two different global analyses.

Parameters		Full scenario	pQCD scenario
δu_v	η_{u_v}	0.928[a]	0.928[a]
	a_{u_v}	0.898 ± 0.022	0.277 ± 0.0072
	b_{u_v}	3.218 ± 0.035	2.725 ± 0.029
	c_{u_v}	3.88[a]	28.95[a]
δd_v	η_{d_v}	−0.342[a]	−0.342[a]
	a_{d_v}	0.217 ± 0.027	0.150 ± 0.012
	b_{d_v}	2.947 ± 1.45	2.591 ± 0.087
	c_{d_v}	9.335[a]	31.75[a]
$\delta_{\bar{q}}$	$\eta_{\bar{q}}$	-0.0288 ± 0.002	-0.0356 ± 0.0033
	$a_{\bar{q}}$	1.227 ± 0.068	1.991 ± 0.041
	$b_{\bar{q}}$	3.364[a]	11.163[a]
	$c_{\bar{q}}$	0.0[a]	0.0[a]
δg	η_g	0.0921 ± 0.022	0.178 ± 0.014
	a_g	10.2 ± 1.22	26.33 ± 0.49
	b_g	46.32[a]	99.95[a]
	c_g	0.0[a]	0.0[a]
$\alpha_s(Q_0^2)$		0.3362 ± 0.002	0.4688 ± 0.0008
χ^2/ndf		1111.789/957 = 1.161	1580.751/957 = 1.651

[a]Those marked with (*) are fixed.

B. Overview of datasets

In our recent analysis which we call it MA22 we focus on the polarized DIS data samples. The required DIS data for all PPDFs are coming from the experiments at electron-proton collider and also in fixed-target including proton, neutron and heavier targets such as deuteron.

TABLE II. Parameter values for the coefficients of the twist-three corrections at $Q^2 = 1$ GeV^2 obtained in the full scenario.

	A	B	C	D	E
$g_{2,p}^{tw-3}$	0.0879	1.0196	−0.8832	−2.3765	2.4234
$g_{2,n}^{tw-3}$	1.0086	0.3009	−0.6583	0.3466	−2.7571
$g_{2,d}^{tw-3}$	0.8878	1.3430	−2.1334	0.1878	2.2293

Although it is not possible to separate quarks from antiquarks, nonetheless it is the inclusive DIS data that are included in the fit. Additionally we take into our MA22 fitting procedure the g_2 structure function. Due to the technical difficulty in operating the required transversely polarized target, these data have been traditionally neglected before.

One of the important quantities which is used as a criteria to indicate the validation of fit, is the chi-square (χ^2) test which is assessing the goodness of fit between observed values and those expected theoretically. We discuss it in the following subsection.

C. χ^2 minimization

The $\chi^2_{\rm global}(\mathrm{p})$ quantifies the goodness of fit to the data for a set of p independent parameters. To determine the best fit, it is needed to minimize the $\chi^2_{\rm global}$ function with the free unknown parameters. We do it for PPDFs at the NNLO approximation which additionally includes the QCD cut off parameter, $\Lambda_{\rm QCD}$ which finally specifies the polarized PDFs at $\mathrm{Q}_0^2 = 1\ \mathrm{GeV}^2$.

This function is presented as it follows:

$$\chi^2_{\rm global}(\mathrm{p}) = \sum_{n=1}^{N_{\rm exp}} w_n \chi^2_n. \tag{19}$$

In this equation, w_n is a weight factor for the nth experiment and χ^2_n is defined by:

$$\chi^2_n(\mathrm{p}) = \left(\frac{1-\mathcal{N}_{\rm n}}{\Delta\mathcal{N}_{\rm n}}\right)^2 + \sum_{\rm i=1}^{\rm N_n^{data}} \left(\frac{\mathcal{N}_{\rm n}\mathrm{g}^{\rm Exp}_{(1,2),\rm i} - \mathrm{g}^{\rm Theory}_{(1,2),\rm i}(\mathrm{p})}{\mathcal{N}_{\rm n}\Delta\mathrm{g}^{\rm Exp}_{(1,2),\rm i}}\right)^2. \tag{20}$$

The minimization of the above $\chi^2_{\rm global}(\mathrm{p})$ function is done using the CERN program library MINUIT [75]. In the above equation, the main contribution comes from the difference between the model and the DIS data within the statistical precision. In the χ^2_n function, $g^{\rm Theory}$ indicates the theoretical value for the ith data point and $g^{\rm Exp}$, $\Delta g^{\rm Exp}$ represent the experimental measurement and the experimental uncertainty (statistical and systematic combined in quadrature) respectively.

To do a proper fit an over normalization factor for the data of experiment n is needed which is denoted by $\mathcal{N}_n$. An uncertainty $\Delta\mathcal{N}_n$ is attributed to this factor which should be considered in the fit. These factors, considering the uncertainties, quoted by the experiments are used to relate different experimental datasets. In fact they are taken as free parameters which are determined simultaneously with the other parameters in the fit. They are obtained in the prefitting procedure and then fixed at their best values in further steps. Numerical results for the unknown parameters, resulted from χ^2 minimization, are listed in Tables I and II. Different datasets which are used in the fit, are presented in Table III.

Now we are at the stage to do some analytical computations for a more confirmation of the fitting validation, taken into account the several sum rules as we do it in the next section.

VII. THE SUM RULES

Sum rules like total momentum fraction carried by partons or the total contribution of parton spin to the spin of the nucleon are important tools to investigate some fundamental properties of the nucleon structure. Inclusion of TMCs and HT terms into the NNLO polarized structure function analysis leads to an improvement for the precision of PPDF determination as well as QCD sum rules and we are exploring herein their effects. In what are following by utilizing available experimental data, we describe some important polarized sum rules.

A. Bjorken sum rule

The polarized Bjorken sum rule expresses the integral over the spin distributions of quarks inside the nucleon in terms of its axial charge, g_A (as measured in neutron β decay), times a coefficient function, $C_{Bj}[\alpha_s(Q^2)]$ [76], and considering higher twist (HT) corrections, it is given by

$$\begin{aligned}\Gamma_1^{\rm NS}(Q^2) &= \Gamma_1^p(Q^2) - \Gamma_1^n(Q^2) \\ &= \int_0^1 [g_1^p(x,Q^2) - g_1^n(x,Q^2)]dx \\ &= \frac{1}{6}|g_A| C_{Bj}[\alpha_s(Q^2)] + \text{HT corrections}.\end{aligned} \tag{21}$$

Bjorken sum rule potentially provides a very precise handle on the α_s as strong coupling constant. The value of coupling can be extracted via $C_{Bj}[\alpha_s(Q^2)]$ expression from experimental data. This function has been calculated in four-loop pQCD corrections in the massless [77] and very recently massive cases [78]. As previously reported in Ref. [79], determination of α_s from the Bjorken sum rule suffers from small-x extrapolation ambiguities.

The α_s is also available form accurate methods to compute the width decay of τ-lepton and the Z-boson into hadrons [80,81]. An important test of QCD consistency can be offered by comparing these values.

Our results for the Bjorken sum rule can be compared with experimental measurements such as E143 [52], SMC [74], HERMES06 [57] and COMPASS16 [59]. The comparisons indicate an adequate consistency as we list them in Table IV.

TABLE III. Summary of published polarized DIS experimental data points with measured x and Q^2 ranges and the number of data points.

Experiment	References	$[x_{\min}, x_{\max}]$	Q^2 (GeV^2)	Number of data points	χ^2	$\mathcal{N}_i$
SLAC/E143(p)	[52]	[0.031–0.749]	1.27–9.52	28	19.0218	0.99705
HERMES(p)	[53]	[0.028–0.66]	1.01–7.36	39	55.2816	0.99982
SMC(p)	[54]	[0.005–0.480]	1.30–58.0	12	8.9328	1.00009
EMC(p)	[55]	[0.015–0.466]	3.50–29.5	10	3.8416	1.00592
SLAC/E155	[56]	[0.015–0.750]	1.22–34.72	24	41.7453	0.99915
HERMES06(p)	[57]	[0.026–0.731]	1.12–14.29	51	21.0559	0.99915
COMPASS10(p)	[58]	[0.005–0.568]	1.10–62.10	15	23.1003	1.00073
COMPASS16(p)	[59]	[0.0035–0.575]	1.03–96.1	54	52.6140	1.00296
SLAC/E143(p)	[52]	[0.031–0.749]	2-3-5	84	122.0060	0.99578
HERMES(p)	[53]	[0.023–0.66]	2.5	20	35.2073	0.99726
SMC(p)	[54]	[0.003–0.4]	10	12	14.8138	1.00071
Jlab06(p)	[60]	[0.3771–0.9086]	3.48–4.96	70	99.6438	1.00127
Jlab17(p)	[61]	[0.37696–0.94585]	3.01503–5.75676	82	171.5716	1.00282
g_1^p				501		
SLAC/E143(d)	[52]	[0.031–0.749]	1.27–9.52	28	38.3735	1.00210
SLAC/E155(d)	[62]	[0.015–0.750]	1.22–34.79	24	20.0319	1.00228
SMC(d)	[54]	[0.005–0.479]	1.30–54.80	12	18.3574	1.00006
HERMES06(d)	[57]	[0.026–0.731]	1.12–14.29	51	44.4642	1.00654
COMPASS05(d)	[63]	[0.0051–0.4740]	1.18–47.5	11	7.3430	1.00760
COMPASS06(d)	[64]	[0.0046–0.566]	1.10–55.3	15	8.4408	1.00052
COMPASS17(d)	[65]	[0.0045–0.569]	1.03–74.1	43	36.2019	1.01090
SLAC/E143(d)	[52]	[0.031–0.749]	2–3–5	84	127.5502	0.99981
g_1^d				268		
SLAC/E142(n)	[66]	[0.035–0.466]	1.10–5.50	8	8.0235	0.99881
HERMES(n)	[53]	[0.033–0.464]	1.22–5.25	9	2.7585	0.99995
E154(n)	[67]	[0.017–0.564]	1.20–15.00	17	14.6888	0.99908
HERMES06(n)	[68]	[0.026–0.731]	1.12–14.29	51	18.1873	0.99913
Jlab03(n)	[69]	[0.14–0.22]	1.09–1.46	4	1.803e-2	0.99950
Jlab04(n)	[70]	[0.33–0.60]	2.71–4.8	3	2.2174	1.05642
Jlab05(n)	[71]	[0.19–0.20]	1.13–1.34	2	3.2639	0.98666
g_1^n				94		
E143(p)	[52]	[0.038–0.595]	1.49–8.85	12	7.1338	1.00074
E155(p)	[72]	[0.038–0.780]	1.1–8.4	8	11.9908	0.99886
Hermes12(p)	[73]	[0.039–0.678]	1.09–10.35	20	22.6010	0.99898
SMC(p)	[74]	[0.010–0.378]	1.36–17.07	6	1.6804	1.00000
g_2^p				46		
E143(d)	[52]	[0.038–0.595]	1.49–8.86	12	8.3504	1.00010
E155(d)	[72]	[0.038–0.780]	1.1–8.2	8	1.9800	1.00296
g_2^d				20		
E143(n)	[52]	[0.038–0.595]	1.49–8.86	12	8.87903	1.00001
E155(n)	[72]	[0.038–0.780]	1.1–8.8	8	6.0324	1.01893
E142(n)	[66]	[0.036–0.466]	1.1–5.5	8	3.8955	0.99999
Jlab03(n)	[69]	[0.14–0.22]	1.09–1.46	4	0.9362	0.99337
Jlab04(n)	[70]	[0.33–0.60]	2.71–4.83	3	3.9915	1.10299
Jlab05(n)	[71]	[0.19–0.20]	1.13–1.34	2	15.5600	0.98986
g_2^n				37		
Total			966		1111.7891	

TABLE IV. Comparison our computed MA22 result for the Bjorken sum rule, Γ_1^{NS}, with world data from E143 [52], SMC [74], HERMES06 [57] and COMPASS16 [59]. Only HERMES06 [57] results are not extrapolated in full x range (measured in region $0.021 \leq x \leq 0.9$).

	E143 [52] $Q^2 = 5$ GeV^2	SMC [74] $Q^2 = 5$ GeV^2	HERMES06 [57] $Q^2 = 5$ GeV^2	COMPASS16 [59] $Q^2 = 3$ GeV^2	KTA17 [13] $Q^2 = 5$ GeV^2	MA22 $Q^2 = 5$ GeV^2
Γ_1^{NS}	0.164 ± 0.021	0.181 ± 0.035	0.148 ± 0.017	0.181 ± 0.008	0.167 ± 0.005	0.171 ± 0.001

B. Proton helicity sum rule

This sum rule is related to the extrapolation of proton spin among its constituents that is completing our knowledge in the field of nuclear physics [82]. An accurate picture of the quark and gluon helicity density are obtained, considering proton's momentum sum rule that needs a precise extraction of PPDFs.

The spin of the nucleon is carried by its constituents that is generally represented by

$$\frac{1}{2} = \frac{1}{2}\Delta\Sigma(Q^2) + \Delta G(Q^2) + L(Q^2). \tag{22}$$

Here $\Delta\Sigma(Q^2) = \sum_i \int_0^1 dx(\Delta q(x, Q^2) + \Delta\bar{q}(x, Q^2))$ denotes spin contribution of the singlet flavor, $\Delta G(Q^2) = \int_0^1 dx \Delta g(x, Q^2)$ is interpreted as the gluon spin contribution and finally $L(Q^2)$ represents the total contribution from quark and gluon orbital angular momentum. Each individual term in Eq. (22) is a function of Q^2 but the sum is not. Finding a way to measure them is a real challenge. Describing the measurement methods is the beyond the scope of this paper.

In Table V the amount of first moment for the singlet-quark and gluon are listed at $Q^2 = 10$ GeV^2. Our results are compared to those from the NNPDFpol1.0 [83], NNPDFpol1.1 [84] and DSSV08 [85] at both truncated and full x region.

In Table VI our results, MA22, are presented and compared with the results of DSSV08 [85], BB10 [47], LSS10 [86], NNPDFpol1.0 [83] and KTA17 [13] at $Q^2 = 4$ GeV^2.

As can be seen from the Tables V and VI for the $\Delta\Sigma$, our MA22 results are consistent, within uncertainty, with those of other groups. It is back to this reason that the first moment of polarized densities are mainly fixed by semi-leptonic decays. Very different values are reported by various groups when we turn to the gluon. Considering their large uncertainty are avoiding us to reach a firm conclusion about the full first moment of gluon.

Based on the extracted values presented in Table VI we can finally discuss the proton spin sum rule. Hence the amount of quark and gluon orbital angular momentum to the spin of the proton would be

$$L(Q^2 = 4 \text{ GeV}^2) = 0.3591 \pm 0.0779. \tag{23}$$

A definite conclusion about the contribution of the total orbital angular momentum to the spin of the proton can not be done because of the large uncertainty that is mainly originating from the gluons. To obtain a precise determination of each individual contribution, it is required to improve the current level of experimental accuracy.

C. The twist-three reduced matrix element d_2

One of the quantities which is not considered as a sum rule but its numerical evaluation is remarkable to investigate the higher twist effect is the twist-three reduced matrix element and is denoted by d_2. Details of higher twist analyses for g_1 polarized structure function have been performed in [47]. In operator product expansion (OPE) theorem [87] the effect of quark-gluon correlations can be studied through the moments of g_1 and g_2 structure functions. These moments lead to definition of reduced matrix element, $d_2(Q^2)$, as it follows

TABLE V. Results for the full and truncated first moments of the polarized singlet-quark $\Delta\Sigma(Q^2) = \sum_i \int_0^1 dx[\Delta q_i(x) + \Delta\bar{q}_i(x)]$ and gluon distributions at the scale $Q^2 = 10$ GeV^2 in the $\overline{\text{MS}}$–scheme. The recent polarized global analysis of NNPDFpol1.0 [83], NNPDFpol1.1 [84], and DSSV08 [85] are also shown.

	DSSV08 [85]	NNPDFpol1.0 [83]	NNPDFpol1.1 [84]	KTA17 [13]	MA22
Full x region [0, 1]					
$\Delta\Sigma(Q^2)$	0.242	$+0.16 \pm 0.30$	$+0.18 \pm 0.21$	0.2587 ± 0.044	0.2445 ± 0.0048
$\Delta G(Q^2)$	-0.084	-0.95 ± 3.87	0.03 ± 3.24	0.2104 ± 0.034	0.1205 ± 0.03
Truncated x region $[10^{-3}, 1]$					
$\Delta\Sigma(Q^2)$	0.366 ± 0.017	$+0.23 \pm 0.15$	$+0.25 \pm 0.10$	0.2661 ± 0.038	0.2551 ± 0.0066
$\Delta G(Q^2)$	0.013 ± 0.182	-0.06 ± 1.12	0.49 ± 0.75	0.2104 ± 0.034	0.1205 ± 0.03

TABLE VI. Same as Table V, but only for the full first moments of the polarized singlet-quark and gluon distributions at the scale $Q_0^2 = 4$ GeV^2 in the $\overline{\text{MS}}$–scheme. Those of DSSV08 [85], BB10 [47], LSS10 [86] and NNPDFpol1.0 [83] are presented for comparison.

	DSSV08 [85]	BB10 [47]	LSS10 [86]	NNPDFpol1.0 [83]	KTA17 [13]	MA22
$\Delta\Sigma(Q^2)$	0.245	0.193 ± 0.075	0.207 ± 0.034	0.18 ± 0.20	0.1774 ± 0.029	0.2607 ± 0.0065
$\Delta G(Q^2)$	−0.096	0.462 ± 0.430	0.316 ± 0.190	-0.9 ± 4.2	0.1882 ± 0.0294	0.1095 ± 0.027

$$d_2(Q^2) = 3\int_0^1 x^2 \bar{g}_2(x,Q^2)dx = \int_0^1 x^2[3g_2(x,Q^2) + 2g_1(x,Q^2)]dx. \quad (24)$$

In this equation $\bar{g}_2 = g_2 - g_2^{WW}$ where g_2^{WW} is given by the Wandzura and Wilczek (WW) relation as in Eq. (3). The $d_2(Q^2)$ that is in fact the twist-three reduced matrix element of spin dependent operators in the nucleon can be used to measure the deviation of g_2 from $g_2^{\tau_2}$. Due to the x^2 weighting factor in Eq. (24), this matrix element is especially sensitive to the large-x behavior of $\bar{g}_2$. Some insights into the size of the multiparton correlation terms can be obtained by extracting the d_2 which indicates its important.

The significance of higher twist terms in QCD analyses is revealed by having nonzero value for d_2. To achieve precise information on the higher twist operators and to improve model prediction, a much more accurate experimental measurement for d_2 is required. In Table VII we present our results for d_2 which are compared with the other theoretical predictions and also experimental values.

D. Burkhardt-Cottingham (BC) sum rule

Considering dispersion relations for virtual Compton scattering in all Q^2, Burkhardt and Cottingham predicted that the zeroth moment of g_2 goes to zero [95] such as:

$$\Gamma_2 = \int_0^1 dx g_2(x,Q^2) = 0. \quad (25)$$

This relation is called Burkhardt-Cottingham (BC) sum rule and is trivial consequence of the WW relation for $g_2^{\tau_2}$ [see Eq. (3)]. It should be noted that zeroth moment of structure function does not exist in the light cone expansion and hence cannot be described by local operator product expansion [96]. Even if the target mass corrected structure function is used, this sum rule is still established [43]. Consequently any violation of the BC sum rule is an evidence for the presence of HT contributions [73].

Our MA22 results for Γ_2 together with data from E143 [52], E155 [72], HERMES2012 [73], RSS [97], E01012 [89] groups for proton, deuteron, and neutron are listed in Table VIII. The low-x behavior of g_2 which is not yet precisely measured, has considerable effect on any conclusion which we might be get.

The BC sum rule can be obtained analytically from the covariant parton model as it is discussed in [98].

E. Efremov-Leader-Teryaev (ELT) sum rule

Considering the valence part of g_1 and g_2 structure functions and integrating them over x variable the Efremov-Leader-Teryaev (ELT) sum rule is obtained. The ELT sum rule is derived like the Bjorken sum rule since the sea quarks are assumed to be identical in protons and neutrons. Hence it appears as:

TABLE VII. d_2 moments of the proton, neutron and deuteron polarized structure functions from the SLAC E155x [88], E01-012 [89], E06-014 [90], Lattice QCD [91], CM bag model [92], JAM15 [93], JAM13 [94], KTA17 [13] compared with MA22 results.

	References	Q^2 [GeV^2]	$10^2 d_2^p$	$10^5 d_2^n$	$10^3 d_2^d$
MA22		5	1.0929 ± 0.0106	209.095 ± 3.96	7.206 ± 0.078
KTA17	[13]	5	0.718 ± 0.01	105.36 ± 74.58	5.16 ± 0.02
E06-014	[90]	3.21		$-421.0 \pm 79.0 \pm 82.0 \pm 8.0$	⋯
E06-014	[90]	4.32		$-35.0 \pm 83.0 \pm 69.0 \pm 7.0$	⋯
E01-012	[89]	3	⋯	$-117 \pm 88 \pm 138$	⋯
E155x	[72]	5	0.32 ± 0.17	790 ± 480	⋯
E143	[52]	5	0.58 ± 0.50	500 ± 2100	5.1 ± 9.2
Lattice QCD	[91]	5	0.4(5)	−100(−300)	⋯
CM bag model	[92]	5	1.74	−253	6.79
JAM15	[93]	1	0.5 ± 0.2	-100 ± 100	⋯
JAM13	[94]	5	1.1 ± 0.2	200 ± 300	⋯

TABLE VIII. Comparison of the result of BC sum rule for Γ_2^p, Γ_2^d, and Γ_2^n with world data from E143 [52], E155 [72], HERMES2012 [73], RSS [97], E01012 [89].

	E143 [52] $0.03 \le x \le 1$ $Q^2 = 5$ GeV^2	E155 [72] $0.02 \le x \le 0.8$ $Q^2 = 5$ GeV^2	HERMES2012 [73] $0.023 \le x \le 0.9$ $Q^2 = 5$ GeV^2	RSS [97] $0.316 < x < 0.823$ $Q^2 = 1.28$ GeV^2	E01012 [89] $0 \le x \le 1$ $Q^2 = 3$ GeV^2	KTA17 [13] $0.03 \le x \le 1$ $Q^2 = 5$ GeV^2	MA22 $0.03 \le x \le 1$ $Q^2 = 5$ GeV^2
Γ_2^p	-0.014 ± 0.028	-0.044 ± 0.008	0.006 ± 0.029	-0.0006 ± 0.0022	...	-0.0196 ± 0.0011	-0.01554 ± 0.00033
Γ_2^d	-0.034 ± 0.082	-0.008 ± 0.012	...	-0.0090 ± 0.0026	...	-0.0036 ± 0.0005	-0.00401 ± 0.00006
Γ_2^n	...	...	...	-0.0092 ± 0.0035	0.00015 ± 0.00113	0.0060 ± 0.0001	0.00721 ± 0.00033

$$\int_0^1 dx x[g_1^V(x) + 2g_2^V(x)] = \int_0^1 dx x[g_1^p(x) - g_1^n(x) + 2(g_2^p(x) - g_2^n(x))] = 0. \quad (26)$$

This sum rule is only valid in the case of massless quarks and receives corrections from the quark mass but under presence of target mass corrections is preserved [96]. Like the BC sum rule, the ELT sum rule can be obtained by analytical considerations of CPM. More details can be found in [98].

By combining the data of E143 [52] and E155 [72] the numerical value for this sum rule at $Q^2 = 5$ GeV^2 is -0.011 ± 0.008 and what we obtain at the same energy scale would be 0.01017 ± 0.00004.

VIII. COMPARISON FOR THE SPIN STRUCTURE FUNCTIONS

Since our QCD analysis has been validated by extracting the PPDFs via the fitting processes and also obtaining their evolved outputs and in continuation by considering several sum rules, we are now at the position to investigate the polarized structure functions. In this regard, we first back to what we got before. Our results, MA22 PPDFs, as a function of x at $Q_0^2 = 1$ GeV^2 along with the corresponding uncertainty bounds, is presented in Fig. 1.

The evolution of MA22 polarized parton distributions for a selection of Q^2 values indicates in Fig. 2 while for comparison various parametrizations of KTA17 [13], KATAO11 [24], TKAA16 [12], NAAMY21 [29] at the NLO approximation are illustrated there. It is seen that by increasing Q^2, except for the gluon density, the evolution of all distributions tends to flatten out the peak.

Now for the structure functions, we see that in different panels of Fig. 3, our MA22 predictions for the polarized structure functions of the proton $xg_1^p(x, Q^2)$, neutron $xg_1^n(x, Q^2)$ and deuteron $xg_1^d(x, Q^2)$ are compared with respect to the fixed-target DIS experimental data from E143. As we mentioned, MA22 refers to "pQCD+TMC +HT" scenario, that is called full scenario. The results from KATAO11 analysis in NLO approximation [24], TKAA16 analysis in NNLO approximation [12], KTA17 analysis in NNLO approximation [13], THK14 analysis in NLO approximation [100] and finally NAAMY21 analysis in NLO approximation [29] are also depicted there. We find our results are in good agreement with the experimental data and in accord with other determinations over the entire range of x at $Q^2 = 5$ GeV^2.

Further illustrations of the fit quality are presented in different panels of Fig. 4, for the $xg_2^{i=p,n,d}(x, Q^2)$ polarized

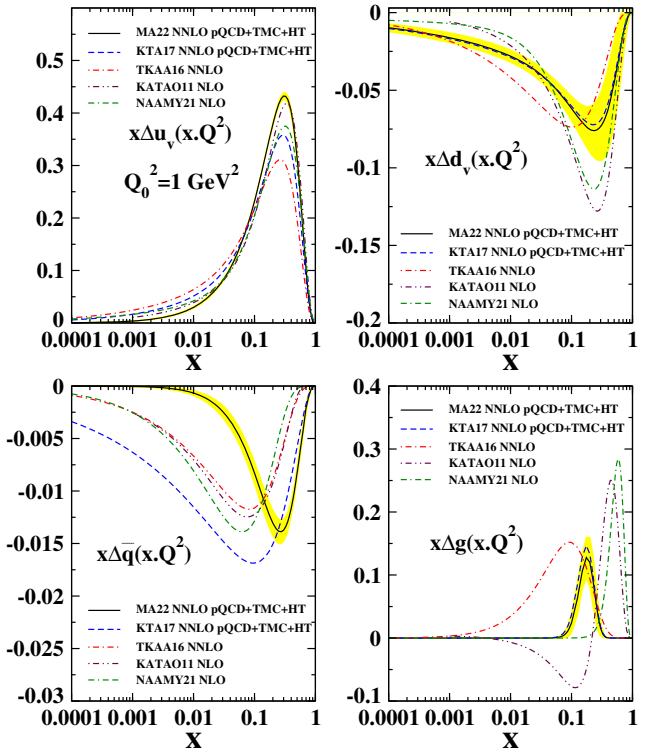

FIG. 1. Our MA22 results for the polarized PDFs at $Q_0^2 = 1$ GeV^2 as a function of x in the NNLO approximation. It is indicated by a solid curve along with their $\Delta\chi^2 = 1$ uncertainty bands which is computed, based on the Hessian approach [99]. The recent results of TKAA16 (dashed-dotted) [12] is also shown in the NNLO approximation without inclusion of HT terms and TMCs. Additionally the KTA17(dashed) [13] in the NNLO approximation is presented including the HT terms and TMCs. The KATAO11(dashed-dotted-dotted) in the NLO approximation [24] is furthermore indicated. Finally the results of NAAMY21 (dashed-dashed-dotted) [29] in the NLO approximation is also plotted.

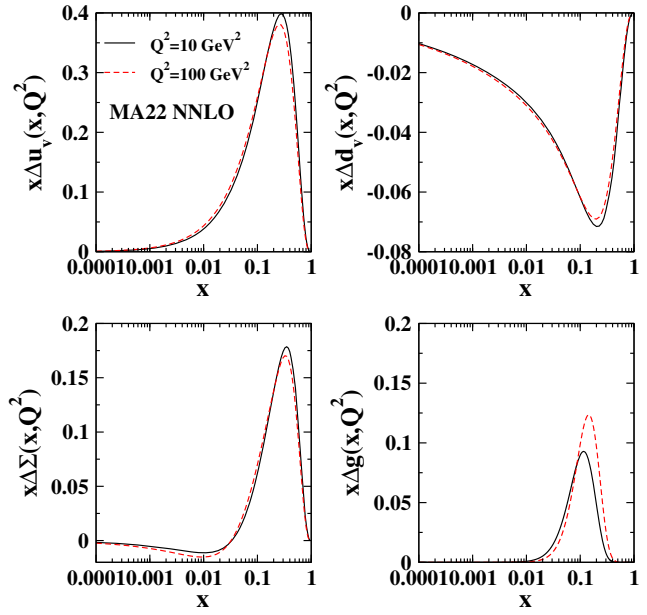

FIG. 2. Our results, MA22 polarized parton distributions as a function of x and for some selected value of $Q^2 = 10, 100\ \mathrm{GeV}^2$.

structure functions, obtained from Eq. (16). In comparison with the g_1 data, the g_2 data have generally larger uncertainties which indicates the lack of knowledge for the g_2 structure function. At the current level of accuracy, MA22 is in agreement with data within their uncertainties. We need a large number of data with higher precision to get a precise quantitative extraction of the $xg_2(x, Q^2)$. In fact we concentrate on the general characteristic of the $xg_2(x, Q^2)$ structure function.

Figure 5 is presenting our MA22 prediction for the polarized structure functions of the proton, $xg_1^p(x, Q^2)$ while a comparison with the fixed-target DIS experimental data from JLAB17 [61] is done there.

Figure 6 represents our $xg_1^{\tau 3}(x, Q^2)$ with the results from LSS [101] and JAM [94] groups. Analysis of the LSS group is based on splitting the measured x region into seven bins to determine the HT correction to g_1. The HT contribution has been extracted by LSS group in a model-independent way while its scale dependence is ignored. On the other side an analytical form for the twist-three part of g_2 is parametrized by the JAM group where using integral relation of Eq. (14) they calculated $g_1^{\tau 3}$ at the NLO accuracy in a global fit.

E143 collaboration at SLAC reported the twist-three contribution to proton spin structure function xg_2^p structure function with relatively large errors [52]. We employ them and present our MA22 results for twist-three part of g_2 in Fig. 7 which are accompanied with those of JAM [94] and BLMP [48] groups.

However, within experimental precision the g_2 data are well described by the twist-two contribution but the precision of the current data is not sufficient enough to distinguish model precision. Hence we compute twist-three part of g_2 for different targets and depict them in Fig. 8 which has significant contribution even at large Q^2 values.

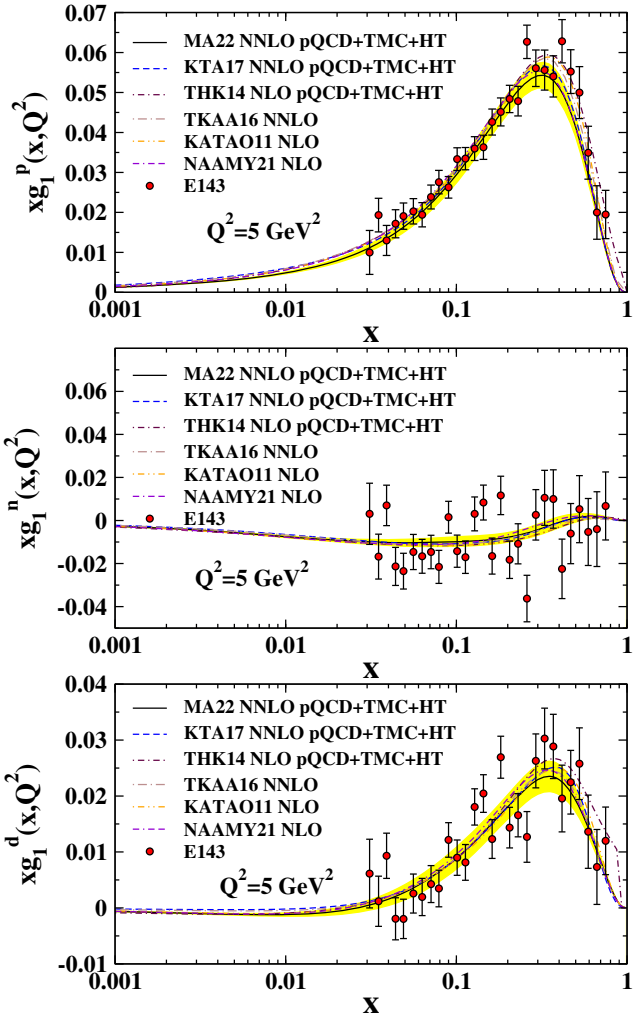

FIG. 3. The spin-dependent proton, neutron, and deuteron structure functions as a function of x and Q^2. Our results, MA22, at the NNLO approximation (solid curve) are compared with KTA17 at the same approximation (dashed) [13], with THK14 at the NLO approximation (dashed-dotted) [100], with TKAA16 at the NNLO approximation (long-dashed dotted) [12], with KATAO11 at the NLO approximation (dashed-dotted-dotted) [24], and finally with NAAMY21 at the NLO approximation (dashed-dashed-dotted) [29].

In continuation to have a comparison, we compute the $xg_1^{\tau_3}$ and indicate them in Fig. 9. We find that these functions vanish rapidly at $Q^2 > 5\ \mathrm{GeV}^2$ where in the limit of $Q^2 \to \infty$, the $xg_2^{\tau_3}$ remains nonzero.

Up here we focused on longitudinal polarized parton densities and structure functions. In next section we utilize our MA22 analysis which we have done before to illustrate the transversal case which are including the polarized TMDs.

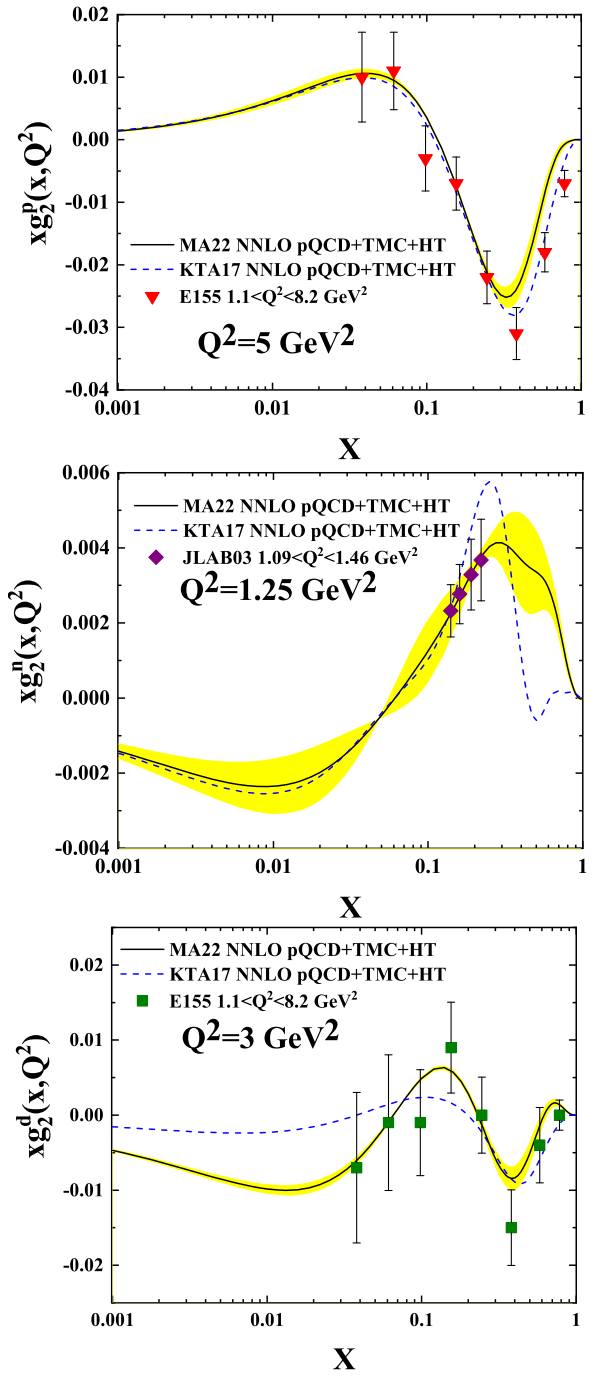

FIG. 4. The spin-dependent proton, neutron and deuteron structure functions, xg_2, as a function of x and Q^2. Our results, MA22, at the NNLO approximation (solid curve) are compared with KTA17 at the same approximation (dashed) [13].

IX. PREDICTIONS FOR POLARIZED TMDs

Since we achieved to sufficient information on longitudinal polarized parton distributions and structure function, we are now at a situation to utilize the covariant parton model [4,102] and extract the transverse momentum dependent (TMD) distributions in polarized case. Indeed

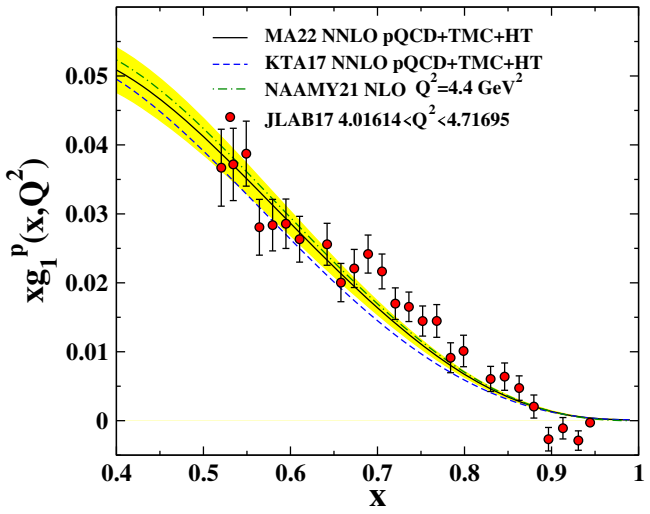

FIG. 5. The spin-dependent proton structure function, xg_1, as a function of x and Q^2. Our result, MA22, at the NNLO approximation (solid curve) is compared with KTA17 at the same approximation (dashed) [13] and with NAAMY21 at the NLO approximation (dashed-dotted) [29].

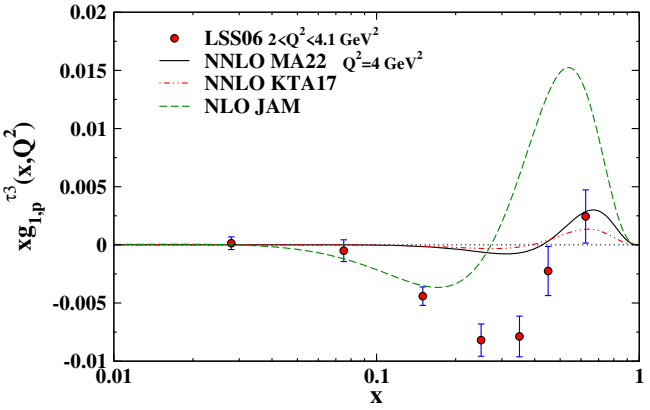

FIG. 6. The twist-three contribution to xg_1^p at $Q^2 = 4$ GeV^2 as a function of x is compared with the results of LSS [101] and KTA17 [13] at NNLO approximation and with JAM [94] at the NLO approximation.

TMDs provide us new insight toward a more complete understanding of the quark-gluon structure in a nucleon [103–109]. Without a more accurate and realistic picture in three dimensions of the nucleon which includes naturally transverse motion, it would be hard to explain some experimental observations. In fact TMDs provide such pictures and their necessities feel more and more in nucleon investigations.

The first and simplest example of quark TMD is $f_1^q(x, k_T)$. It arises when an unpolarized beam scatters off an unpolarized target hadron, and therefore does not carry quark/hadron spin information. The function $f_1^q(x, k_T)$ provides the probability that a beam particle strikes a target quark of momentum fraction x and

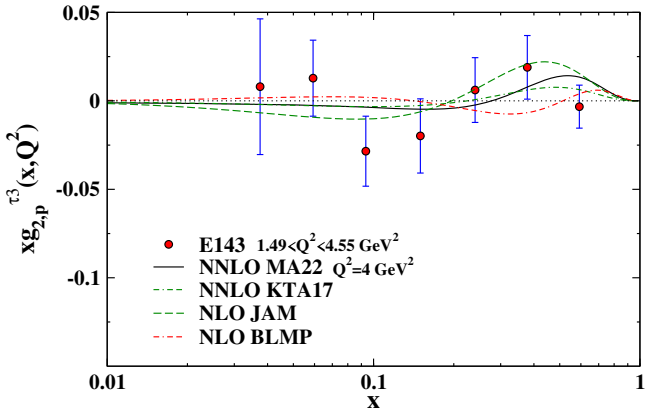

FIG. 7. The twist-three contribution to xg_2^p at $Q^2 = 4$ GeV^2 as a function of x. Our result, MA22 (solid curve), is compared with KTA17 at the NNLO approimation [13](dashed-dotted), JAM [94](dashed) and BLMP [48] (dashed dashed dotted) at the NLO approximation. E143 experimental data [52] have also been added.

transverse momentum k_T. It is related to the traditional DIS PDF $f_1^q(x)$ by $\int d^2k_T f_1^q(x,k_T) = f_1^q(x)$.

Similarly to $f_1^q(x,k_T)$, we get the $g_1^q(x,k_T)$ as longitudinal polarized TMD and $h_1^q(x,k_T)$ as transverse

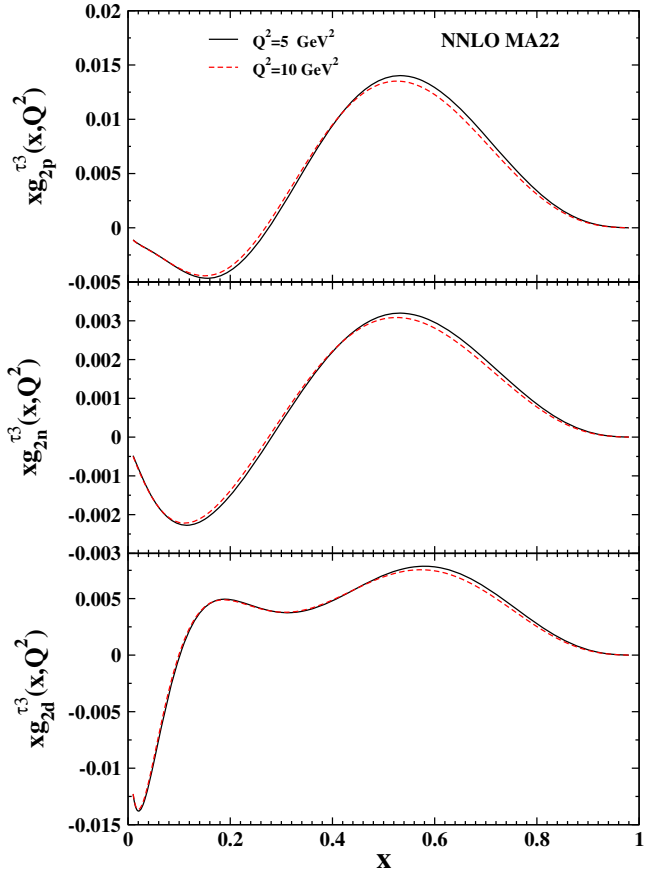

FIG. 8. The twist-three contribution of xg_2 for the proton, neutron, and deuteron as a function of x and for different values of Q^2 according to our result, MA22, at the NNLO analysis.

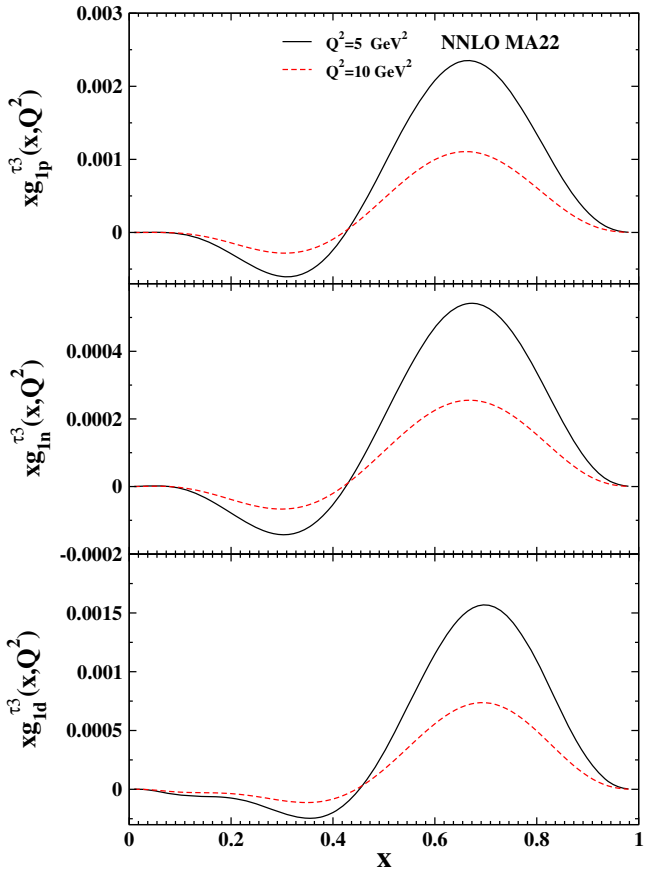

FIG. 9. The twist-three contribution of xg_1 for the proton, neutron, and deuteron as a function of x and for different values of Q^2 according to our results, MA22, at the NNLO analysis.

polarized TMD, whose integrals are denoted respectively by $g_1^q(x)$ [presented before by $\Delta q_i(x)$] and $h_1^q(x)$ that we know them as quark longitudinal polarized (helicity) distribution and the quark transversity distribution.

In addition to the three above TMDs for quarks which are direct extension of the DIS PDFs, there are five other quark TMDs which depend not only on the magnitude of k_T, but also on its direction. Therefore these TMDs vanish if simply integrated over k_T, and do not directly connect to DIS PDFs. They are

(1) The Sivers distribution $f_{1T}^{\perp,q}$ which expresses, in a transversely polarized hadron, the asymmetric distribution of the quark transverse momentum, p_z, around the center of the p_x and p_y plane [110]. The appearance of azimuthal asymmetric quark distribution in the transverse momentum space is often called the "Sivers effect." This TMD has opposite signs in semi-inclusive DIS (SIDIS) with respect to Drell-Yan processes and it is therefore an odd time reversal function(T-odd function).

(2) The Boer-Mulders function $h_1^{\perp,q}(x,k_T)$ characterizes the distribution of longitudinal polarized quarks in an unpolarized hadron [111]. It is also a T-odd function, like $f_{1T}^{\perp,q}$. The rest tree TMDs are

(3) Function $h_{1T}^{\perp,q}(x,k_T)$ which is describing a transverse polarized quark inside a transverse polarized nucleon while its direction is perpendicular to a polarized nucleon. It is called the pretzelosity function.
(4) Function $g_{1T}^{\perp,q}(x,k_T)$ that is describing the longitudinal polarized quark inside a transverse polarized nucleon and is named as Worm-gear-I function. And finally:
(5) Worm-gear-II function, denoted by $h_{1L}^{\perp,q}(x,k_T)$ and is describing the transverse polarized quark inside a longitudinal polarized nucleon,

Similarly to quark TMDs, gluon TMDs allow access to the gluonic orbital angular momentum, another possibly important contribution to the nucleon spin. Just as there are eight TMDs for quarks, there are eight gluon TMDs [112]. Gluon TMDs were first proposed in 2001 [113].

Here we only consider the quark TMDs that are twist-two naively and time-reversal even (T-even) functions. They have been extracted via the covariant parton model (CPM) which is based on the Lorentz invariance and the assumption of a rotationally symmetric distribution of parton momenta in the nucleon rest frame [114]. From now on to liken and equalize the symbol for transverse momentum with other literatures, we utilize p_T instead of k_T.

As a result of CPM, T-even polarized TMDs can be obtained at the leading twist approximation, in terms of a single "generating function" $K^q(x,\mathbf{p}_T)$. They are given by [115,116]

$$\begin{aligned}
g_1^q(x,\mathbf{p}_T) &= \frac{1}{2x}\left(\left(x+\frac{m}{M}\right)^2-\frac{\mathbf{p}_T^2}{M^2}\right)\times K^q(x,\mathbf{p}_T),\\
h_1^q(x,\mathbf{p}_T) &= \frac{1}{2x}\left(x+\frac{m}{M}\right)^2\times K^q(x,\mathbf{p}_T),\\
g_{1T}^{\perp,q}(x,\mathbf{p}_T) &= \frac{1}{x}\left(x+\frac{m}{M}\right)\times K^q(x,\mathbf{p}_T),\\
h_{1L}^{\perp,q}(x,\mathbf{p}_T) &= -\frac{1}{x}\left(x+\frac{m}{M}\right)\times K^q(x,\mathbf{p}_T),\\
h_{1T}^{\perp,q}(x,\mathbf{p}_T) &= -\frac{1}{x}\times K^q(x,\mathbf{p}_T).
\end{aligned} \tag{27}$$

According to [114]) $K^q(x,\mathbf{p}_T)$ as generating function is defined in compact notation by

$$K^q(x,\mathbf{p}_T) = M^2 x\int \mathrm{d}\{p^1\} \tag{28}$$

$$\mathrm{d}\{p^1\} \equiv \frac{\mathrm{d}p^1}{p^0}\frac{H^q(p^0)}{p^0+m}\delta\left(\frac{p^0+p^1}{M}-x\right). \tag{29}$$

It can be shown that due to rotational symmetry the following relations hold [115]:

$$K^q(x,\mathbf{p}_T) = M^2\frac{H^q(\bar{p}^0)}{\bar{p}^0+m},\quad \bar{p}^0=\frac{1}{2}xM\left(1+\frac{\mathbf{p}_T^2+m^2}{x^2M^2}\right), \tag{30}$$

$$\pi x^2M^3H^q\left(\frac{M}{2}x\right) = 2\int_x^1\frac{\mathrm{d}y}{y}g_1^q(y)+3g_1^q(x)-x\frac{\mathrm{d}g_1^q(x)}{\mathrm{d}x}. \tag{31}$$

In deriving Eq. (31) the limit $m\to 0$ has been taken. Consequently the following result in that limit would be obtained for the generating function [115]:

$$\begin{aligned}
K^q(x,\mathbf{p}_T) &= \frac{H^q(\frac{M}{2}\xi)}{\frac{M}{2}\xi}\\
&= \frac{2}{\pi\xi^3M^4}\left(2\int_\xi^1\frac{\mathrm{d}y}{y}g_1^q(y)+3g_1^q(\xi)-x\frac{\mathrm{d}g_1^q(\xi)}{\mathrm{d}\xi}\right),\\
\xi &= x\left(1+\frac{\mathbf{p}_T^2}{x^2M^2}\right).
\end{aligned} \tag{32}$$

Substituting the above relations in Eq. (27), the following result for the $g_1^q(x,\mathbf{p}_T)$ would be obtained:

$$g_1^q(x,\mathbf{p}_T) = \frac{2x-\xi}{\pi\xi^3M^3}\left(2\int_\xi^1\frac{\mathrm{d}y}{y}g_1^q(y)+3g_1^q(\xi)-\xi\frac{\mathrm{d}g_1^q(\xi)}{\mathrm{d}\xi}\right). \tag{33}$$

Based on above relation and using the MA22 analysis which we did in this paper for $g_1^q(x)$ at 4 GeV^2 in the NNLO approximation, we could obtain the result for $g_1^q(x,\mathbf{p}_T)$ which has been shown in Fig. 10 for u and d quarks.

Using Eq. (27) and in the limit $m\to 0$ the other TMDs can be obtained. They are presented in below which which are different by simple x-dependent prefactors [115]:

$$\begin{aligned}
h_1^q(x,\mathbf{p}_T) &= \frac{x}{2}K^q(x,\mathbf{p}_T),\\
g_{1T}^{\perp,q}(x,\mathbf{p}_T) &= K^q(x,\mathbf{p}_T),\\
h_{1T}^{\perp,q}(x,\mathbf{p}_T) &= -\frac{1}{x}K^q(x,\mathbf{p}_T).
\end{aligned} \tag{34}$$

The result for $h_1^q(x,\mathbf{p}_T)$ is depicted in Fig. 11. In Fig. 12 the result for $g_{1T}^{\perp q}$ with respect to x and p_T/M is shown. It does not need to plot $h_{1L}^{\perp q}$ since in the used approach this TMD is equal to $-g_{1T}^{\perp q}$ [114]. As can be seen from Fig. 10, $g_1^q(x,\mathbf{p}_T)$ is the only TMD which has positive and negative values. The other TMDs in other figures do not change sign which follows from Eqs. (27), (34).

We should note that among all TMDs, as we see from Fig. 13, $h_{1T}^{\perp q}(x,\mathbf{p}_T)$ as the pretzelosity function has the largest absolute value which is due to the prefactor $1/x$.

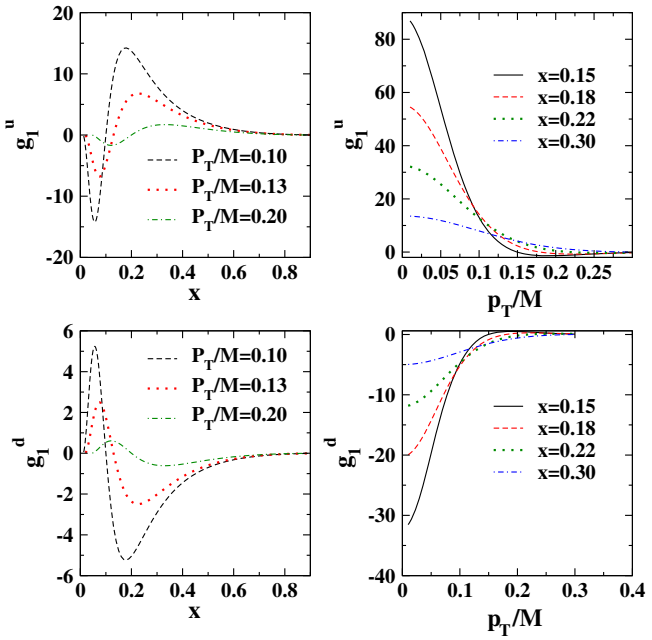

FIG. 10. The TMD $g_1^q(x,\mathbf{p}_T)$ for u- (upper panel) and d-quarks (lower panel). Left panel: $g_1^q(x,\mathbf{p}_T)$ as function of x for $p_T/M = 0.10$ (dashed), 0.13 (dotted), 0.20 (dash-dotted line). Right panel: $g_1^q(x,\mathbf{p}_T)$ as function of p_T/M for $x = 0.15$ (solid), 0.18 (dashed), 0.22 (dotted), 0.30 (dash-dotted line).

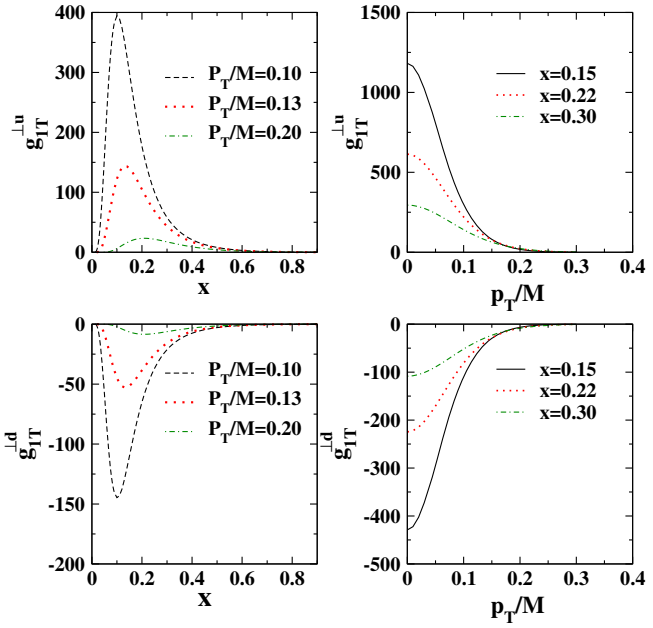

FIG. 12. $g_{1T}^{\perp q}(x,\mathbf{p}_T)$, for u- and d-quarks. Left panel: the TMDs as functions of x for $p_T/M = 0.10$ (dashed), 0.13 (dotted), 0.20 (dash-dotted lines). Right panel: the TMDs as functions of p_T/M for $x = 0.15$ (solid), 0.22 (dotted), 0.30 (dash-dotted lines).

This function has its own worth since in some quark models [117,118], including the utilized approach in [119,120], this function is related to quark orbital angular momentum.

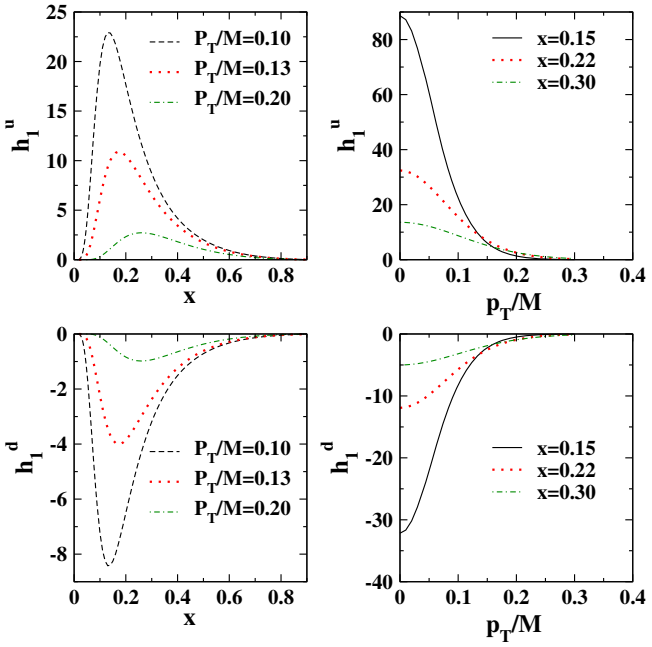

FIG. 11. $h_1^q(x,\mathbf{p}_T)$, for u- and d-quarks. Left panel: the TMDs as functions of x for $p_T/M = 0.10$ (dashed), 0.13 (dotted), 0.20 (dash-dotted lines). Right panel: the TMDs as functions of p_T/M for $x = 0.15$ (solid), 0.22 (dotted), 0.30 (dash-dotted lines).

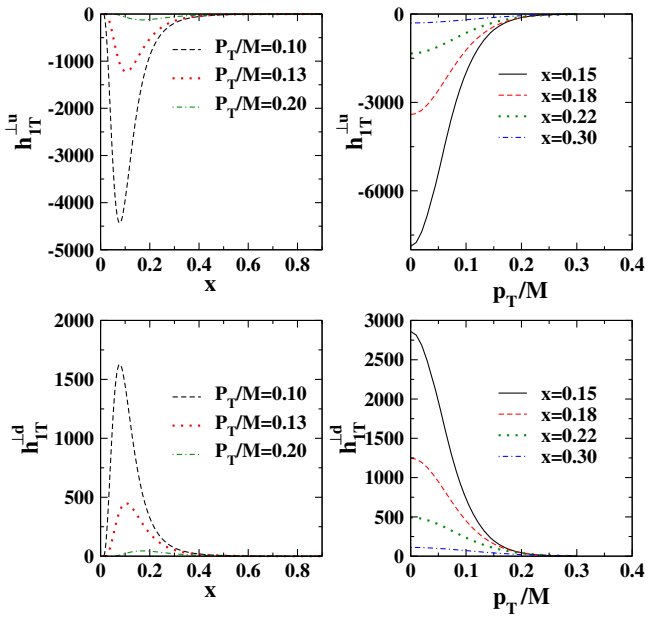

FIG. 13. $h_{1T}^{\perp q}(x,\mathbf{p}_T)$ for u- and d-quarks. Left panel: the TMDs as functions of x for $p_T/M = 0.10$ (dashed), 0.13 (dotted), 0.20 (dash-dotted lines). Right panel: the TMDs as functions of p_T/M for $x = 0.15$ (solid), 0.18 (dashed), 0.22 (dotted), 0.30 (dash-dotted lines).

X. CONCLUSIONS

Determining the nucleon spin structure functions $g_1(x, Q^2)$ and $g_2(x, Q^2)$ and their moments is the main goal of our present MA22 analysis. They are essential to test QCD sum rules and to evaluate the TMDs. We provided a unified and consistent PPDF through an achievement, containing an excellent description of the fitted data while we employed TMC and HT effects in our analysis. Within the known very large uncertainties arising from the lack of constraining data, our helicity distributions are in good consistency with other extractions. Here the TMCs and HT effects, which are relevant in the region of low Q^2, have also been studied for the several sum rules at the NNLO approximation. Our results for the reduced matrix element d_2 at the NNLO approximation have also been presented. We also studied Burkhardt-Cottinghan and Efremov-Leader-Teryaev sum rules. To scrutinize them, more accurate data are needed.

Finally we studied the behavior of the TMD structure functions which are time-reversal even with respect to x and p_T/M variables at the NNLO approximation, based on the covariant parton model. Our MA22 results, containing analysis of up to date and last data on nucleon spin structure functions, with respect to what we did in [13], can be compared with the results from [115] which indicated adequate and acceptable behaviors.

This study can be extended to include other TMDS while higher twist effect is employed. We hope to report on this issue in our further research.

The available data which we use in our recent analysis are up to date and including more data than we employed in our pervious analysis [13]. In fact we use all available g_1^p data from E143, HERMES98, SMC, EMC, E155, HERMES06, COMPASS10, COMPASS16, JLAB06, and JLAB17 experiments [52–61], and g_1^n data from HERMES98, E142, E154, HERMES06, Jlab03, Jlab04, and Jlab05 [53,66–71] and finally the g_1^d data from E143, SMC, HERMES06, E155, COMPASS05, COMPASS06, and COMPASS17 [52,54,57,62–65]. The DIS data for $g_2^{p,n,d}$ from E143, E142, Jlab03, Jlab04, Jlab05, E155, Hermes12, and SMC [52,66,69–74] also are included. These datasets are summarized in Table III. The kinematic coverage, the number of data points for each given target, and the fitted normalization shifts $\mathcal{N}_i$ also presented in this table. Our MA22 analysis algorithm computes the Q^2 evolution and extracts the structure function in x space using Jacobi polynomials approach. It corresponds to the fitting programs on the market which solve the Dokshitzer-Gribov-LipatovAltarelli-Parisi (DGLAP) evolution equations in the Mellin space.

ACKNOWLEDGMENTS

The authors are indebted P. Zavda for reading the manuscript and providing useful comments. We are grateful to O. V. Treyaev for his useful comments and suggestion. We are appreciated P. Schweitzer for reading our manuscript and giving us his opinion about it. S. A. T. is thankful from the School of Particles and Accelerators, Institute for Research in Fundamental Sciences (IPM) to make the required facilities to do this project. A. M. acknowledges the Yazd university for the provided facility to do this project.

[1] C. Thorn, Phys. Rev. D **19**, 639 (1979).
[2] C. Bouchiat, P. Fayet, and P. Meyer, Nucl. Phys. **B34**, 157 (1971).
[3] P. V. Landshoff and J. C. Polkinghorne, Phys. Rep. **5**, 1 (1972).
[4] P. Zavada, Eur. Phys. J. C **52**, 121 (2007).
[5] M. Anselmino, M. Boglione, and F. Murgia, Phys. Lett. B **362**, 164 (1995).
[6] A. Kotzinian, Nucl. Phys. **B441**, 234 (1995).
[7] H. Mahdizadeh Saffar, A. Mirjalili, M. M. Yazdanpanah, and S. Atashbar Tehrani, Int. J. Mod. Phys. A **32**, 1750175 (2017).
[8] J. D. Jackson, G. G. Ross, and R. G. Roberts, Phys. Lett. B **226**, 159 (1989).
[9] R. G. Roberts and G. G. Ross, Phys. Lett. B **373**, 235 (1996).
[10] J. Blumlein and N. Kochelev, Phys. Lett. B **381**, 296 (1996).
[11] S. J. Brodsky, D. S. Hwang, and I. Schmidt, Phys. Lett. B **530**, 99 (2002).
[12] F. Taghavi-Shahri, H. Khanpour, S. Atashbar Tehrani, and Z. Alizadeh Yazdi, Phys. Rev. D **93**, 114024 (2016).
[13] H. Khanpour, S. T. Monfared, and S. Atashbar Tehrani, Phys. Rev. D **95**, 074006 (2017).
[14] Y. Goto, N. Hayashi, M. Hirai, H. Horikawa, S. Kumano, M. Miyama, T. Morii, N. Saito, T.-A. Shibata, E. Taniguchi, and T. Yamanishi (Asymmetry Analysis Collaboration), Phys. Rev. D **62**, 034017 (2000).
[15] S. Moch, J. A. M. Vermaseren, and A. Vogt, Nucl. Phys. **B889**, 351 (2014).
[16] J. Blümlein, P. Marquard, C. Schneider, and K. Schönwald, J. High Energy Phys. 01 (2022) 193.
[17] J. Blümlein, P. Marquard, C. Schneider, and K. Schönwald, Nucl. Phys. **B971**, 115542 (2021).
[18] B. Lampe and E. Reya, Phys. Rep. **332**, 1 (2000).

[19] E. B. Zijlstra and W. L. van Neerven, Nucl. Phys. **B417**, 61 (1994); **B426**, 245 (1994); **B501**, 599 (1997); **B773**, 105 (2007).
[20] M. Lacombe, B. Loiseau, R. Vinh Mau, J. Cote, P. Pires, and R. de Tourreil, Phys. Lett. **101B**, 139 (1981).
[21] W. W. Buck and F. Gross, Phys. Rev. D **20**, 2361 (1979).
[22] M. J. Zuilhof and J. A. Tjon, Phys. Rev. C **22**, 2369 (1980).
[23] S. Wandzura and F. Wilczek, Phys. Lett. **72B**, 195 (1977).
[24] A. N. Khorramian, S. Atashbar Tehrani, S. Taheri Monfared, F. Arbabifar, and F. I. Olness, Phys. Rev. D **83**, 054017 (2011).
[25] A. N. Khorramian, H. Khanpour, and S. A. Tehrani, Phys. Rev. D **81**, 014013 (2010).
[26] S. M. Moosavi Nejad, H. Khanpour, S. Atashbar Tehrani, and M. Mahdavi, Phys. Rev. C **94**, 045201 (2016).
[27] H. Khanpour, A. Mirjalili, and S. Atashbar Tehrani, Phys. Rev. C **95**, 035201 (2017).
[28] S. Atashbar Tehrani, F. Taghavi-Shahri, A. Mirjalili, and M. M. Yazdanpanah, Phys. Rev. D **87**, 114012 (2013); **88**, 039902(E) (2013).
[29] H. Nematollahi, P. Abolhadi, S. Atashbar, A. Mirjalili, and M. M. Yazdanpanah, Eur. Phys. J. C **81**, 18 (2021).
[30] C. Ayala and S. V. Mikhailov, Phys. Rev. D **92**, 014028 (2015).
[31] I. S. Barker, B. R. Martin, and G. Shaw, Z. Phys. C **19**, 147 (1983).
[32] I. S. Barker and B. R. Martin, Z. Phys. C **24**, 255 (1984).
[33] V. G. Krivokhizhin, S. P. Kurlovich, V. V. Sanadze, I. A. Savin, A. V. Sidorov, and N. B. Skachkov, Z. Phys. C **36**, 51 (1987).
[34] V. G. Krivokhizhin, S. P. Kurlovich, R. Lednicky, S. Nemecek, V. V. Sanadze, I. A. Savin, A. V. Sidorov, and N. B. Skachkov, Z. Phys. C **48**, 347 (1990).
[35] J. Chyla and J. Rames, Z. Phys. C **31**, 151 (1986).
[36] I. S. Barker, C. S. Langensiepen, and G. Shaw, Nucl. Phys. **B186**, 61 (1981).
[37] A. L. Kataev, A. V. Kotikov, G. Parente, and A. V. Sidorov, Phys. Lett. B **417**, 374 (1998).
[38] S. I. Alekhin and A. L. Kataev, Phys. Lett. B **452**, 402 (1999).
[39] A. L. Kataev, G. Parente, and A. V. Sidorov, Nucl. Phys. **B573**, 405 (2000).
[40] A. L. Kataev, G. Parente, and A. V. Sidorov, Fiz. Elem. Chastits At. Yadra **34**, 43 (2003) [Phys. Part. Nucl. **34**, 20 (2003)]; **38**, 827 (2007).
[41] A. L. Kataev, Pis'ma Zh. Eksp. Teor. Fiz. **81**, 744 (2005) [JETP Lett. **81**, 608 (2005)].
[42] E. Leader, A. V. Sidorov, and D. B. Stamenov, Int. J. Mod. Phys. A **13**, 5573 (1998).
[43] J. Blumlein and A. Tkabladze, Nucl. Phys. **B553**, 427 (1999).
[44] H. Georgi and H. D. Politzer, Phys. Rev. D **14**, 1829 (1976).
[45] J. Blumlein and A. Tkabladze, Nucl. Phys. B, Proc. Suppl. **79**, 541 (1999).
[46] O. Nachtmann, Nucl. Phys. **B63**, 237 (1973).
[47] J. Blumlein and H. Bottcher, Nucl. Phys. **B841**, 205 (2010).
[48] V. M. Braun, T. Lautenschlager, A. N. Manashov, and B. Pirnay, Phys. Rev. D **83**, 094023 (2011).
[49] J. Blumlein and H. Bottcher, arXiv:1207.3170.
[50] M. Tanabashi *et al.* (Particle Data Group), Phys. Rev. D **98**, 030001 (2018).
[51] P. A. Zyla *et al.* (Particle Data Group), Prog. Theor. Exp. Phys. **2020**, 083C01 (2020).
[52] K. Abe *et al.* (E143 Collaboration), Phys. Rev. D **58**, 112003 (1998).
[53] A. Airapetian *et al.* (HERMES Collaboration), Phys. Lett. B **442**, 484 (1998).
[54] B. Adeva *et al.* (Spin Muon Collaboration), Phys. Rev. D **58**, 112001 (1998).
[55] J. Ashman *et al.* (European Muon Collaboration), Phys. Lett. B **206**, 364 (1988).
[56] P. L. Anthony *et al.* (E155 Collaboration), Phys. Lett. B **493**, 19 (2000).
[57] A. Airapetian *et al.* (HERMES Collaboration), Phys. Rev. D **75**, 012007 (2007).
[58] M. G. Alekseev *et al.* (COMPASS Collaboration), Phys. Lett. B **690**, 466 (2010); V. Y. Alexakhin *et al.* (COMPASS Collaboration), Phys. Lett. B **647**, 8 (2007).
[59] C. Adolph *et al.* (COMPASS Collaboration), Phys. Lett. B **753**, 18 (2016).
[60] K. V. Dharmawardane *et al.* (CLAS Collaboration), Phys. Lett. B **641**, 11 (2006).
[61] R. Fersch *et al.* (CLAS Collaboration), Phys. Rev. C **96**, 065208 (2017).
[62] P. L. Anthony *et al.* (E155 Collaboration), Phys. Lett. B **463**, 339 (1999).
[63] E. S. Ageev *et al.* (COMPASS Collaboration), Phys. Lett. B **612**, 154 (2005).
[64] V. Y. Alexakhin *et al.* (COMPASS Collaboration), Phys. Lett. B **647**, 8 (2007).
[65] C. Adolph *et al.* (COMPASS Collaboration), Phys. Lett. B **769**, 34 (2017).
[66] P. L. Anthony *et al.* (E142 Collaboration), Phys. Rev. D **54**, 6620 (1996).
[67] K. Abe *et al.* (E154 Collaboration), Phys. Rev. Lett. **79**, 26 (1997).
[68] K. Ackerstaff *et al.* (HERMES Collaboration), Phys. Lett. B **404**, 383 (1997).
[69] K. M. Kramer (Jefferson Lab E97-103 Collaboration), AIP Conf. Proc. **675**, 615 (2003).
[70] X. Zheng *et al.* (Jefferson Lab Hall A Collaboration), Phys. Rev. C **70**, 065207 (2004).
[71] K. Kramer, D. S. Armstrong, T. D. Averett, W. Bertozzi, S. Binet, C. Butuceanu, A. Camsonne, G. D. Cates *et al.*, Phys. Rev. Lett. **95**, 142002 (2005).
[72] P. L. Anthony *et al.* (E155 Collaboration), Phys. Lett. B **553**, 18 (2003).
[73] A. Airapetian, N. Akopov, Z. Akopov, E. C. Aschenauer, W. Augustyniak, R. Avakian, A. Avetissian, E. Avetisyan *et al.*, Eur. Phys. J. C **72**, 1921 (2012).
[74] D. Adams *et al.* (Spin Muon (SMC) Collaboration), Phys. Rev. D **56**, 5330 (1997).
[75] F. James and M. Roos, Comput. Phys. Commun. **10**, 343 (1975).
[76] J. D. Bjorken, Phys. Rev. D **1**, 1376 (1970).

[77] P. A. Baikov, K. G. Chetyrkin, and J. H. Kuhn, Phys. Rev. Lett. **104**, 132004 (2010).
[78] J. Blümlein, G. Falcioni, and A. De Freitas, Nucl. Phys. **B910**, 568 (2016).
[79] G. Altarelli, R. D. Ball, S. Forte, and G. Ridolfi, Acta Phys. Pol. B **29**, 1145 (1998).
[80] M. Akrami and A. Mirjalili, Phys. Rev. D **99**, 074023 (2019).
[81] M. Akrami and A. Mirjalili, Phys. Rev. D **101**, 034007 (2020).
[82] E. Leader, arXiv:1604.00305.
[83] R. D. Ball, S. Forte, A. Guffanti, E. R. Nocera, G. Ridolfi, and J. Rojo (NNPDF Collaboration), Nucl. Phys. **B874**, 36 (2013).
[84] E. R. Nocera, S. Forte, G. Ridolfi, and J. Rojo, arXiv: 1206.0201.
[85] D. de Florian, R. Sassot, M. Stratmann, and W. Vogelsang, Phys. Rev. Lett. **101**, 072001 (2008).
[86] E. Leader, A. V. Sidorov, and D. B. Stamenov, Phys. Rev. D **82**, 114018 (2010).
[87] J. C. Collins, *Renormalization: An Introduction to Renormalization, the Renormalization Group and the Operator-Product Expansion* (Cambridge University Press, Cambridge, England, 1984).
[88] S. E. Kuhn, J. P. Chen, and E. Leader, Prog. Part. Nucl. Phys. **63**, 1 (2009).
[89] P. Solvignon *et al.* (E01-012 Collaboration), Phys. Rev. C **92**, 015208 (2015).
[90] D. Flay *et al.*, Phys. Rev. D **94**, 052003 (2016).
[91] M. Gockeler, R. Horsley, D. Pleiter, P. E. L. Rakow, A. Schafer, G. Schierholz, H. Stuben, and J. M. Zanotti, Phys. Rev. D **72**, 054507 (2005).
[92] X. Song, Phys. Rev. D **54**, 1955 (1996).
[93] N. Sato, W. Melnitchouk, S. E. Kuhn, J. J. Ethier, and A. Accardi (Jefferson Lab Angular Momentum Collaboration), Phys. Rev. D **93**, 074005 (2016).
[94] P. Jimenez-Delgado, A. Accardi, and W. Melnitchouk, Phys. Rev. D **89**, 034025 (2014).
[95] H. Burkhardt and W. N. Cottingham, Ann. Phys. (N.Y.) **56**, 453 (1970).
[96] J. Blumlein and N. Kochelev, Nucl. Phys. **B498**, 285 (1997).
[97] K. Slifer *et al.* (Resonance Spin Structure Collaboration), Phys. Rev. Lett. **105**, 101601 (2010).
[98] P. Zavada, Phys. Rev. D **65**, 054040 (2002).
[99] J. Pumplin, D. Stump, R. Brock, D. Casey, J. Huston, J. Kalk, H. L. Lai, and W. K. Tung, Phys. Rev. D **65**, 014013 (2001).
[100] S. Taheri Monfared, Z. Haddadi, and A. N. Khorramian, Phys. Rev. D **89**, 074052 (2014); **89**, 119901(E) (2014).
[101] E. Leader, A. V. Sidorov, and D. B. Stamenov, Phys. Rev. D **75**, 074027 (2007).
[102] A. V. Efremov, P. Schweitzer, O. V. Teryaev, and P. Zavada, Phys. Rev. D **83**, 054025 (2011).
[103] J. C. Collins, Acta Phys. Pol. B **34**, 3103 (2003).
[104] J. C. Collins, T. C. Rogers, and A. M. Stasto, Phys. Rev. D **77**, 085009 (2008).
[105] J. C. Collins and F. Hautmann, Phys. Lett. B **472**, 129 (2000).
[106] J. C. Collins and F. Hautmann, J. High Energy Phys. 03 (2001) 016.
[107] F. Hautmann, Phys. Lett. B **655**, 26 (2007).
[108] P. J. Mulders and R. D. Tangerman, Nucl. Phys. **B461**, 197 (1996); **B484**, 538(E) (1997).
[109] A. Bacchetta, M. Diehl, K. Goeke, A. Metz, P. J. Mulders, and M. Schlegel, J. High Energy Phys. 02 (2007) 093.
[110] D. Sivers, Phys. Rev. D **41**, 83 (1990).
[111] D. Boer and P. J. Mulders, Phys. Rev. D **57**, 5780 (1998).
[112] S. Meissner, A. Metz, and K. Goeke, Phys. Rev. D **76**, 034002 (2007).
[113] S. Meissner, P. J. Mulders, and J. Rodrigues, Phys. Rev. D **63**, 094021 (2007).
[114] A. V. Efremov, P. Schweitzer, O. V. Teryaev, and P. Zavada, Phys. Rev. D **80**, 014021 (2009).
[115] A. V. Efremov, P. Schweitzer, O. V. Teryaev, and P. Zavada, J. Phys. Conf. Ser. **295**, 012052 (2011).
[116] S. Bastami, A. V. Efremov, P. Schweitzer, O. V. Teryaev, and P. Zavada, Phys. Rev. D **103**, 014024 (2021).
[117] J. She, J. Zhu, and B. Q. Ma, Phys. Rev. D **79**, 054008 (2009).
[118] H. Avakian, A. V. Efremov, P. Schweitzer, and F. Yuan, Phys. Rev. D **81**, 074035 (2010).
[119] A. V. Efremov, P. Schweitzer, O. V. Teryaev, and P. Zavada, Proc. Sci. DIS2010 (**2010**) 253 [arXiv:1008.3827].
[120] H. Avakian, A. V. Efremov, P. Schweitzer, O. V. Teryaev, and P. Zavada, arXiv:1008.1921.